ChemPubSoc Europe

DOI: 10.1002/celc.201901650

CHEMELECTROCHEM Articles

Special Issue

Single-Site, Single-Metal-Atom, Heterogeneous Electrocatalyst: Metal–Organic-Framework Supported Molybdenum Sulfide for Redox Mediator-Assisted Hydrogen Evolution Reaction

Hyunho Noh[+],[a] Ying Yang[+],[a] Xuan Zhang,[a] Timothy A. Goetjen,[a] Zoha H. Syed,[a] Zhiyong Lu,[a, c] Sol Ahn,[b] Omar K. Farha,[a, b] and Joseph T. Hupp*[a]

Dedicated to Prof. Richard M. Crooks on the occasion of his 65th birthday

Synthesis of single-site catalysts, whereby the local structure and surrounding chemical environments are identical, has been challenging, particularly in heterogeneous catalysis, as the support often presents spectrum of chemically distinct binding sites. Yet, the above criteria are crucial in attributing the apparent catalytic performance to the structural motif. The presented work augments on our previous work using *monometallic* molybdenum sulfide tethered within a zirconium-based metal-organic framework (MOF), NU-1000; the *monometallic* nature enables all presented sites to be catalytically addressable. As the molybdenum sulfide species resided within two distinct pores (micro- and mesopores) of the MOF support, we have imparted uniformity in the local chemical environment by reducing the pore heterogeneity down to a single mesopore. Single-site and single-atom nature of the candidate catalyst was established via X-ray diffraction measurements. Redox mediators were implemented, which, under reductive potentials, provide reduced species; they can effectively deliver the necessary reducing equivalences to the catalytic units that can otherwise not be addressed electrochemically due to the low electron mobility within the framework. Our results indicate the micropore-allocated molybdenum sulfide is approximately four times more active as that in mesopores, whereas its catalytic mechanism is identical, underscoring the importance of controlling chemical environment beyond the active site.

1. Introduction

As an essential chemical feedstock for Fisher-Tropsch,[1–3] Haber-Bosch,[4–5] and many other processes, molecular hydrogen plays a critical role in modern chemical transformations. Current reliance on methane steam reforming or coal gasification to yield H_2 produces substantial amounts of greenhouse gases,[6] CO and/or CO_2, either as a co-product with H_2 or through fossil fuel combustion to achieve the necessary temperature and pressure. With the increasing demand for limiting, or ideally, eliminating greenhouse gas emission,[7] it is evident that widespread adoption of an alternative and more sustainable process that is carbon-neutral, is of paramount importance.

In this context, photo-,[8–10] electro-,[11–12] or photoelectrochemical[13] reduction of water (or hydronium ions) to molecular hydrogen, *i.e.*, the hydrogen evolution reaction (HER), is ideal. Coupling HER to the corresponding oxidative reaction, namely molecular oxygen evolution, yields overall water splitting, and thus, molecular hydrogen formation in a carbon-neutral manner. Current *state-of-the-art* HER electrocatalysts are composed of platinum and/or other precious metals;[14] they all exhibit nearly optimal bond energies for metal-hydrogen(atom) intermediates, *i.e.* combined energies that, at the thermodynamic potential for hydrogen evolution, nearly match those of reactants ($2H^+ + 2e^-$) and of product, H_2. The close matching translates into small activation energies and large exchange-current densities. The scarcity and expense of these elements, however, militate against their widespread use to produce H_2.

Metal chalcogenides, most commonly sulfides and the selenides, have been *in-silico* predicted[15–16] and experimentally validated[17–19] as alternative HER electrocatalysts with activity approaching that of platinum. Of those, molybdenum disulfide, in layered two-dimensional form, is perhaps the most extensively examined for HER. Among the most important findings is that crystallographic edge sites with undercoordinated molybdenum atoms (which during catalysis form molybdenum-hydride species) resulted in a significant enhancement of catalytic performance.[15,17] A common approach for increasing the fraction of edge sites has been amorphization of molybdenum disulfide, which enriches the catalyst exterior with these undercoordinated molybdenum species.[19–20] However, amorph-

[a] H. Noh,[+] Y. Yang,[+] Dr. X. Zhang, T. A. Goetjen, Z. H. Syed, Dr. Z. Lu, Prof. O. K. Farha, Prof. J. T. Hupp
Department of Chemistry, Northwestern University
2145 Sheridan Rd., Evanston, IL 60208 (USA)
E-mail: j-hupp@northwestern.edu
[b] S. Ahn, Prof. O. K. Farha
Department of Chemical and Biological Engineering, Northwestern University
2145 Sheridan Rd., Evanston, IL 60208 (USA)
[c] Dr. Z. Lu
College of Mechanics and Materials, Hohai University, Nanjing 210098, China
[+] These authors contributed equally to this work.

Supporting information for this article is available on the WWW under https://doi.org/10.1002/celc.201901650

Special Issue An invited contribution to the Richard M. Crooks Festschrift

© 2019 Wiley-VCH Verlag GmbH & Co. KGaA, Weinheim

21960216, 2020, 2, Downloaded from https://chemistry-europe.onlinelibrary.wiley.com/doi/10.1002/celc.201901650 by Chung-Ang University, Wiley Online Library on [26/11/2024]. See the Terms and Conditions (https://onlinelibrary.wiley.com/terms-and-conditions) on Wiley Online Library for rules of use; OA articles are governed by the applicable Creative Commons License

ization comes with the cost of structural ambiguity and heterogeneity of the catalytic sites, impeding the deduction of structure-activity relationships.

Recently, chemists have realized the virtue of using metal-organic frameworks (MOFs) as a heterogeneous support[21–24] to yield single-site, or near single-site catalysts,[11,25–28] owing to its periodic displacement of the two constituents, the inorganic node and the organic linker. In particular, we have recently reported a *monometallic* molybdenum disulfhydryl unit ($Mo(SH)_2$) post-synthetically incorporated onto the hexanuclear oxozirconium-based node of the MOF, NU-1000.[11] NU-1000 presents hierarchical microporous and mesoporous channels constructed by the Zr_6 node and *1,3,5,8*-(*p*-benzoate)pyrene linker ($TBAPy^{4-}$); see Figure 1.[31] The node of the parent framework presents labile protons in the form of ligated hydroxo and aqua groups.[32] The protons are readily displaceable upon introducing reactive metal precursors (molecular complexes) either through a vapor-phase (in an atomic layer deposition-like process)[33–34] or condensed-phase reaction.[11,35–38]

Molybdenum sulfide was deposited onto the node through solution-phase SIM (**s**olvothermal **i**nstallation in **M**OFs) of Mo (VI) ions[38–39] followed by a gas-phase H_2S treatment at elevated temperature, leading to a simultaneous reduction of Mo(VI) to (IV) and displacement of two oxy ligands by sulfhydryl ligands. The resulting material, named **MoS_x-SIM**, was found to be electrocatalytically active for hydrogen evolution in aqueous acid upon introduction of redox mediators (RMs), *i.e.*, molecular species that can readily diffuse through the porous MOF and deliver electrons from the underlying conductive-glass electrode to the catalysts. The mediators are needed because the MOF itself is electrically insulating at the potentials relevant for hydrogen evolution. As illustrated in Figure 1, the structure of MoS_x-SIM was unambiguously resolved through single-crystal X-ray diffraction measurements. All units are *monometallic* (*i.e.*, contain a single metal atom) and structurally resemble the aforementioned undercoordinated molybdenum sites.[11] As evident from Figure 1, the $Mo(SH)_2$ units are allocated to both the hexagonal mesoporous channel (*ca.* 27 Å diameter after Mo $(SH)_2$ installation) and geometrically orthogonal microporous channels (henceforth referred to as *c*-pores; the pore width is below 10 Å after $Mo(SH)_2$ installation).

Note that while the structures of the variously sited $Mo(SH)_2$ units are essentially identical, the hexagonal mesopore and the channel-connecting micropore (*c*-pore) constitute chemically distinct catalyst environments. An intriguing and unresolved question is whether the differing environments translate into differing degrees of activity for hydrogen evolution for otherwise identical monometallic catalysts. Siting at the perimeter mesopore directs the catalyst toward a broad solvent-filled channel. Siting in the *c*-pore directs the node-bound catalyst toward aqua and hydroxo ligands on the node defining the opposite wall of the pore. While not immediately proximal to

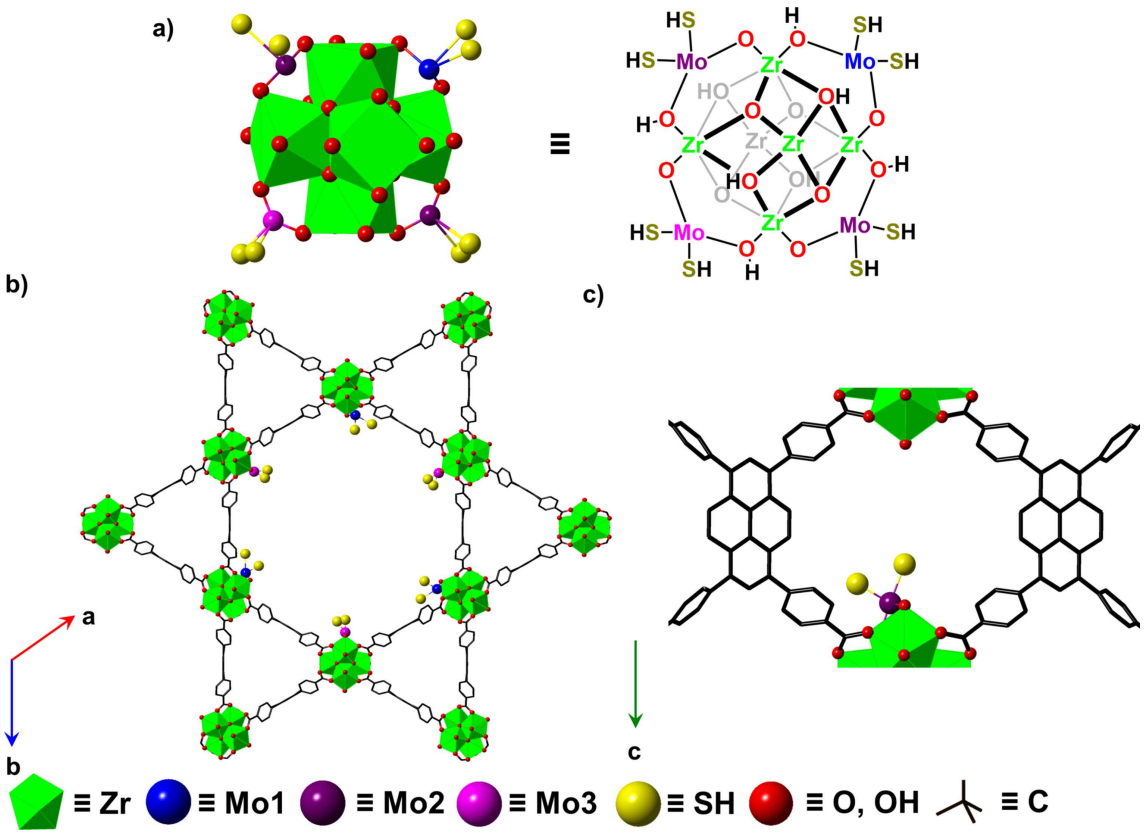


Figure 1. Crystal structure showing the **a)** functionalized Zr_6 node, **b)** hexagonal mesopore and trigonal micropore,[29] and **c)** microporous *c*-pore of **MoS_x-SIM**.[30] Three crystallographically distinct types of Mo(IV) atoms are differentiated by color (**Mo1-3**) and the arrows indicate the three crystallographic axes. Note that the sites are only partially occupied, such that the average number of $Mo(SH)_2$ units per node is 2.6 ± 0.2. For details, see Ref. [11].

© 2019 Wiley-VCH Verlag GmbH & Co. KGaA, Weinheim

the catalyst, these ligands are sufficiently close that communication via hydrogen-bonding to intervening water and/or hydronium ions can be envisioned; see Figure 1.

We reasoned that the ambiguity about site-specific catalytic activity could be eliminated by preemptively blocking single-metal-atom catalyst installation in one of the two pore environments. Specifically, we explore here the use in NU-1000 of naphthalene dicarboxylate (NDC) as a site-directing agent for SIM-based installation of $Mo(SH)_2$ species. Peters *et al.*[40] have

shown crystallographically that NDC, when introduced via solvent-assisted ligand incorporation (SALI),[41] exclusively occupies the *c*-pore (in the limit of one NDC per node). The preference for the *c*-pore can be understood as arising from the uniquely ditopic mode of binding here (as opposed to monotopic binding in the mesopores). When incorporated in this fashion, NDC blocks the *c*-pore, and should cause subsequently installed $Mo(SH)_2$ units to be allocated to a single type of a MOF pore, namely the mesopore. We show here that site-selective allocation is indeed obtained. The resulting material, hereafter referred to as **MoS_x-SIM-NDC-SALI**, has been evaluated an HER electrocatalyst. Outlined below is its activity as a function of pH, RM concentration, RM formal potential (E_f), and reactant isotopic (H/D) composition. The combined results, when compared with those obtained for the NDC-free version of the MOF supported catalyst, allow for assessment of pore-environment effects upon the catalytic activity of otherwise identical, single-metal-atom electrocatalysts.

2. Results and Discussion

2.1. MoS_x-SIM-NDC-SALI Characterization

NDC incorporation *via* SALI, Mo(VI) oxide deposition and the subsequent reduction to (IV), and sulfidation were performed on the parent framework, NU-1000, according to the reported procedures.[11,38,40,42] The resulting material, **MoS_x-SIM-NDC-SALI**, retained its porosity after the above treatments, as evident from the N_2 adsorption-desorption isotherm performed at 77 K; see Figure 2a. The Brunauer-Emmett-Teller (BET) area of the oxide derivative, **MoO_x-SIM-NDC-SALI** and **MoS_x-SIM-NDC-SALI** are comparable to that without **NDC-SALI** (**Table S1**). The N_2-isotherm-derived, density functional theory (DFT)-calculated pore size distribution further revealed the pore sizes to be similar to that reported previously in the absence of NDC (Figure S1).[11,38] ^1H NMR of the digested samples all suggest that throughout all post-synthetic treatments, NDC was retained to be *ca.* one per Zr_6 node, corresponding to the expected value if it were to bridge two Zr_6 nodes across the *c*-pore; see Figure S2 and Table S2.[40]

The valence states of Mo in **MoO_x-SIM-NDC-SALI** and **MoS_x-SIM-NDC-SALI** were confirmed by X-ray absorption spectroscopy (XAS); namely in the X-ray absorption near edge structure (XANES) region the edge energies correlate well with the corresponding Mo(VI) oxide and Mo(IV) sulfide standards. (Figure S3a). A pronounced pre-edge feature is present in spectra for oxide-based samples and suggests tetrahedral local symmetry.[43–44] For bulk MoS_2, this feature is absent, as the

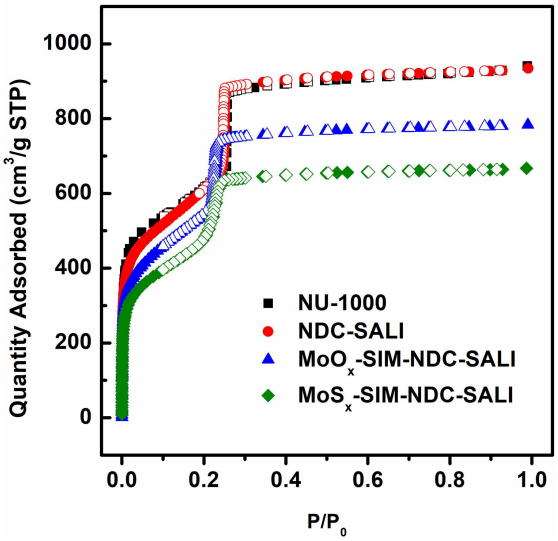


Figure 2. N_2 adsorption-desorption isotherm of NU-1000, **NDC-SALI**, **MoO_x-SIM-NDC-SALI**, and **MoS_x-SIM-NDC-SALI**. The filled and unfilled shapes indicate the adsorption and desorption, respectively.

trigonal prismatic coordination of Mo (with an inversion center)[45] makes the 1 s-to-4d transition symmetry-forbidden. In the XANES spectrum of **MoS_x-SIM-NDC-SALI**, however, the pre-edge feature is recovered, suggesting retention of tetrahedral coordination (or at least the lack of an inversion center).-Coordination to S-based ligands is further evidenced by the extended X-ray absorption fine structure (EXAFS) spectra of **MoO_x-SIM-NDC-SALI** and **MoS_x-SIM-NDC-SALI**; sulfidation shifts primary scattering peak shifts from 1.2 to 1.9 Å (Figure S3b), correlating well with EXAFS results for corresponding oxide and sulfide standards, respectively. The absence in all MOF-based samples of secondary scattering peaks otherwise prominent in bulk materials like MoS_2 (*i.e.*, peaks due to Mo–Mo-metal scattering) suggests that grafted species exist in very small nuclearity (*i.e.*, single or few Mo atoms). The S 2p X-ray photoelectron spectrum (XPS) of **MoS_x-SIM-NDC-SALI** confirmed the oxidation state of ligated sulfur to be 2-(Figure S4). Inductively-coupled plasma optical emission spectroscopy (ICP-OES) measurements showed the number of Mo atoms per Zr_6 node and the number of S atoms per Mo atom ratios to be 2.3 ± 0.3 and 2.3 ± 0.2, respectively. These loadings are similar to those previously reported for NDC-free samples.[11]

Single-crystal X-ray diffraction was used to determine the structure of **MoS_x-SIM-NDC-SALI** the atomic-level of precision. Evident from Figures 3a–c are the following: (a) NDC incorporation prior to Mo installation indeed causes molybdenum sulfide to be allocated exclusively to the perimeter of the hexagonal mesopore of the MOF framework, (b) molybdenum sulfide exists as node-grafted, monometallic $Mo(SH)_2$ units, and (c) the $Mo(SH)_2$ units are structurally identical to those reported previously[11] for NDC-free NU-1000 where such units were allocated to both the mesopore and the *c*-pore. Finally, the mesopore-sited $Mo(SH)_2$ units partially occupy two equivalent positions, designated previously (see Figure 1) as Mo1 and Mo3. Thus, single-crystal X-ray results

© 2019 Wiley-VCH Verlag GmbH & Co. KGaA, Weinheim

21960216, 2020, 2, Downloaded from https://chemistry-europe.onlinelibrary.wiley.com/doi/10.1002/celc.201901650 by Chung-Ang University, Wiley Online Library on [26/11/2024]. See the Terms and Conditions (https://onlinelibrary.wiley.com/terms-and-conditions) on Wiley Online Library for rules of use; OA articles are governed by the applicable Creative Commons License

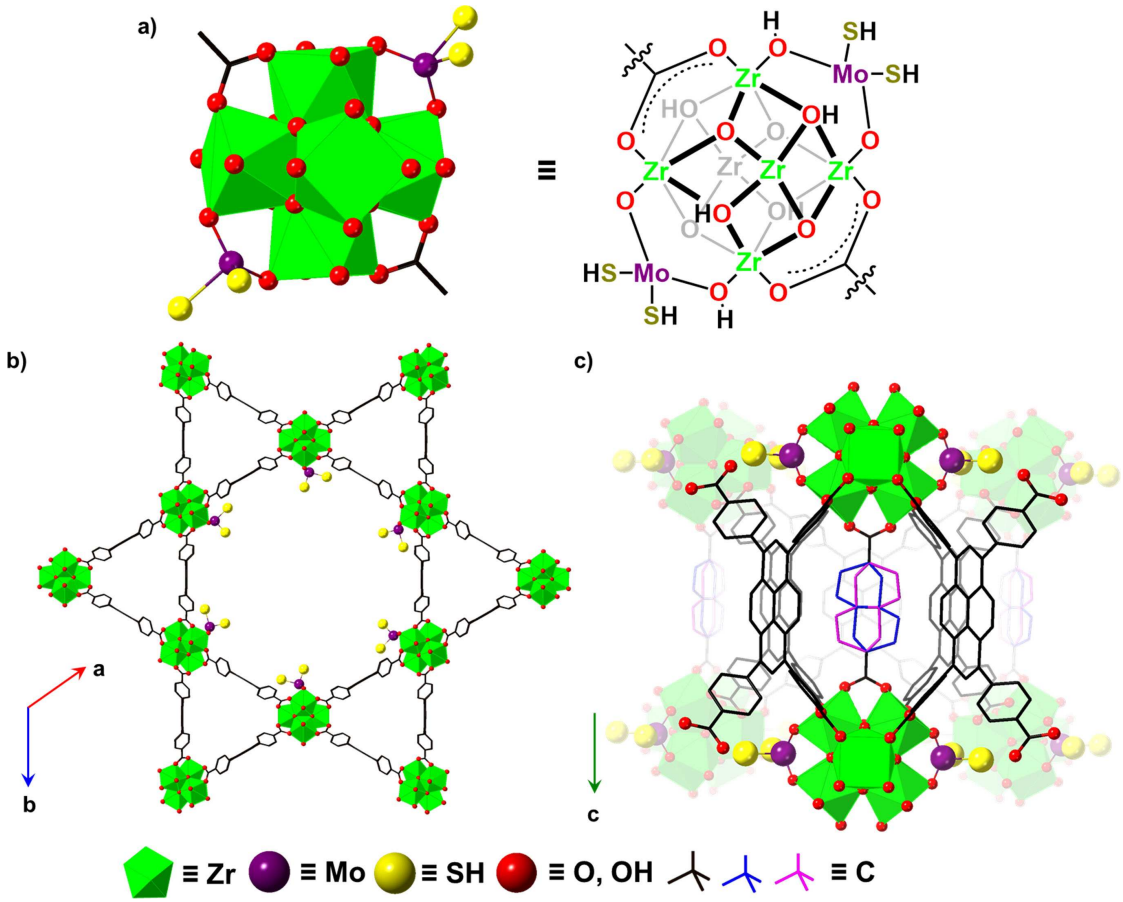


Figure 3. Crystallographic structure of **MoS_x-SIM-NDC-SALI** where **a)** shows the Zr_6 node with monometallic $Mo(SH)_2$ units allocated solely within the mesopore due to the NDC installation (truncated for clarity). **b)** and **c)** are **MoS_x-SIM-NDC-SALI** viewed along the hexagonal mesopore and micropore occupied by NDC (with disorder indicated by two separate colors) along the crystallographic *c*- and *a*-axes (indicated by the arrows), respectively.

establish that **MoS_x-SIM-NDC-SALI** indeed presents a porous, MOF-supported array of single-site, single-metal-atom candidate catalysts (see **Table S3** for further details). Here, we use the term "single-site" exclusively to mean that all catalytic units within a material, regardless of the metal-nuclearity of the units, are: a) identical in structure and chemical composition, b) identically chemically and structurally supported, and c) subjected to identical environments. Thus, catalytic units in Figure 1 satisfy requirements *a* and *b*, but not *c*, whereas those in Figure 3 satisfy all three requirements.

2.2. Electrocatalytic Hydrogen Evolution

With structural results in hand for both **MoS_x-SIM-NDC-SALI** and NDC-free **MoS_x-SIM** we initiated studies of their performance in aqueous acid as electrocatalysts for hydrogen evolution. As shown in Figure S5, cyclic voltammetry (CV) measurements in aqueous H_2SO_4 at pH 1.2, in the absence of a redox mediator, yielded similar results – with only marginal indications of molybdenum-sulfide based electrocatalysis. Bulk electrolysis experiments at −420 mV vs. the reversible hydrogen electrode (RHE) yielded detectable H_2 for **MoS_x-SIM-NDC-SALI** as a catalyst, but not for control samples (FTO, NU-1000, **NDC-SALI**, and **MoO_x-SIM-NDC-SALI**). The average turnover frequency (TOF) of **MoS_x-SIM-NDC-SALI** was measured to be extremely low: 0.17 ± 0.03 min^{-1}. (TOFs were calculated on the basis of all Mo species present in the film determined through ICP-OES and UV-Vis measurements of a decomposed film; see the **Supporting Information** for details.) We interpret the low TOF value as arising from lack of participation of the vast majority of the installed catalysts – which in turn reflects the insulating character of the catalyst support, *i.e.* the porous MOF, at −420 mV.[11]

2.3. Redox Mediator-Assisted Electrocatalysis

We have previously shown that otherwise electrically isolated, MOF-supported catalysts can be enlisted for hydrogen evolution by introducing molecular redox mediators, most notably methyl viologen (MV^{2+}) with E_f of −360 mV vs. RHE.[46] As evidenced by the CV data in Figure 4a, the control samples **MoO_x-SIM-NDC-SALI**, **NDC-SALI**, NU-1000, and bare conductive substrate (fluorine-doped tin oxide or FTO) remain incapable of performing HER at *ca.* −0.4 to −0.5 V in the presence of 10 mM of MV^{2+}. In contrast, **MoS_x-SIM-NDC-SALI** showed significant enhancement in its

© 2019 Wiley-VCH Verlag GmbH & Co. KGaA, Weinheim

21960216, 2020, 2, Downloaded from https://chemistry-europe.onlinelibrary.wiley.com/doi/10.1002/celc.201901650 by Chung-Ang University, Wiley Online Library on [26/11/2024]. See the Terms and Conditions (https://onlinelibrary.wiley.com/terms-and-conditions) on Wiley Online Library for rules of use; OA articles are governed by the applicable Creative Commons License

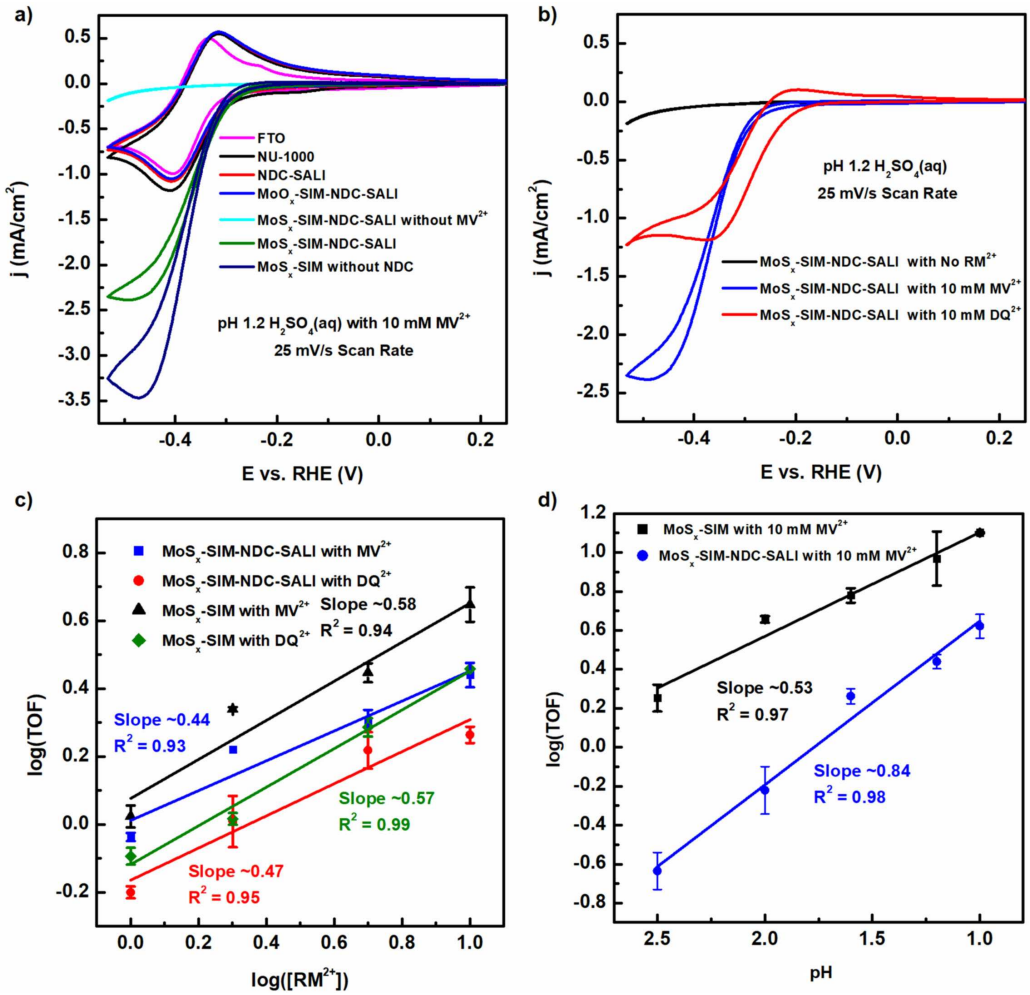


Figure 4. a) CVs of FTO, NU-1000, **NDC-SALI**, **MoO_x-SIM-NDC-SALI**, **MoS_x-SIM-NDC-SALI**, and **MoS_x-SIM** without NDC with 10 mM MV^{2+} in the electrolyte. CV taken with **MoS_x-SIM-NDC-SALI**, but with no MV^{2+} is shown for comparison. **b)** CVs of **MoS_x-SIM-NDC-SALI** with no RM^{2+}, 10 mM MV^{2+}, or 10 mM DQ^{2+} in the electrolyte. **c)** log(TOF) vs. log([RM^{2+}]) and **d)** log(TOF) vs. pH plots deduced from bulk electrolysis at −420 mV vs. RHE where the slope indicates the apparent reaction order with respect to RM^{2+} and proton concentrations, respectively.

catalytic current reaching *ca.* 2.5 mA/cm^2 at −500 mV vs. RHE. Intriguingly, however, the observed current was measured to be lower than if the electrode was instead fabricated with **MoS_x-SIM** in the absence of NDC, despite both systems presenting nearly equal $Mo(SH)_2$ units per node, and consequently, the absolute amount of catalytic sites within both films are nearly identical. Powder X-ray diffraction patterns in Figure S6 confirm the retention of the crystalline framework during all post-synthetic treatments (NDC installation, MoO_x deposition, sulfidation, electrode fabrication, and after bulk electrolysis). ICP-OES measurement after catalysis revealed no loss of Mo.

We further aimed to deduce how the catalytic rate scales as a function of the formal potential of the RMs, by instead employing diquat (DQ^{2+}) with E_f of −289 mV vs. RHE.[46] As revealed by the CVs in Figure 4b, the onset potential for electrocatalysis is less negative, but the magnitude of the plateau current for electrocatalysis is diminished. These observations indicate that $DQ^{2+/\bullet+}$ is functional as a redox mediator, but suggest that the rate of electron transfer (ET) from the reduced mediator to the catalyst limits to at least some extent the overall rate of hydrogen evolution, since the decrease in plateau current density occurs when the driving force for mediator-to-catalyst ET is decreased (in this case by ~80 mV). The voltammetric findings regarding the dependence on of catalyst performance on mediator identity are mirrored decreases by constant-potential electrolysis assessments of H_2 TOFs (Figure 4c). By varying the concentrations of the two RMs, the apparent fractional reaction order with respect to the bulk mediator concentration was observed, as shown in Figure 4c (for CVs and chronoamperometric curves taken during the bulk electrolysis, see Figures S7 and S8). We previously attributed this to the mediator participation in the rate-determining step (RDS; *i.e.,* RM-assisted electron transfer(s) are part of, or precede, the RDS) when (a) electrogenerated $RM^{\bullet+}$ exists in a steady state and (b) due to the highly reductive potential applied, the concentration of the oxidized species, RM^{2+}, exists in a substantially lower concentration than the reduced analogue. Though electrocatalysis clearly occurs, the active-sites in **MoS_x-SIM-NDC-SALI** display smaller TOFs than do the active-sites in the more environmentally diverse, NDC-free **MoS_x-SIM** material.

© 2019 Wiley-VCH Verlag GmbH & Co. KGaA, Weinheim

21960216, 2020, 2, Downloaded from https://chemistry-europe.onlinelibrary.wiley.com/doi/10.1002/cetc.201901650 by Chung-Ang University, Wiley Online Library on [26/11/2024]. See the Terms and Conditions (https://onlinelibrary.wiley.com/terms-and-conditions) on Wiley Online Library for rules of use; OA articles are governed by the applicable Creative Commons License

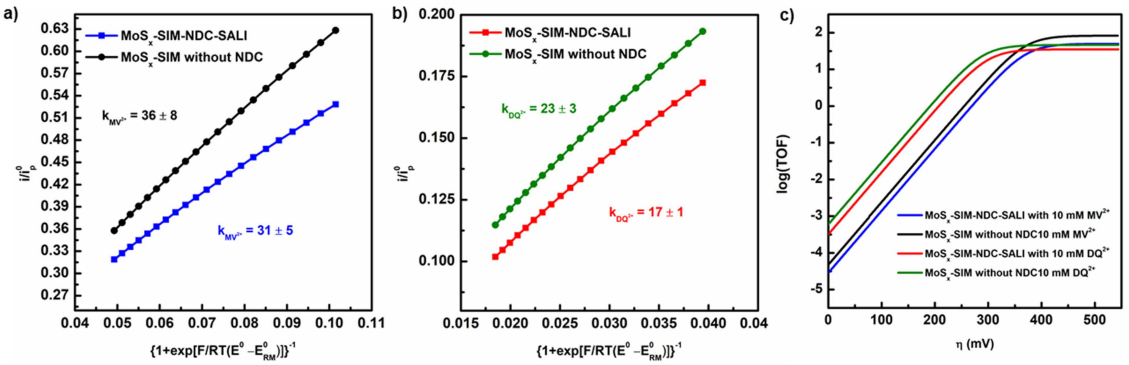


Figure 5. Foot-of-the-wave analysis on **MoS_x-SIM-NDC-SALI** and the analogous system without NDC where the deduced slopes from **a)** and **b)** were used to calculate the corresponding second-order rate constants for the two redox mediators, and further used to calculate **c)** log(TOF) *vs.* overpotential plots.

Faradaic efficiencies (FEs) calculated at all above concentrations further suggest that in the presence of MV^{2+} the values are consistently higher than those when instead DQ^{2+} is present (Figure S9).[47] Given the larger thermodynamic driving force in electron transfer of $MV^{\bullet+}$ as to $DQ^{\bullet+}$, evident from their difference in formal potentials, FEs of DQ-assisted systems were measured to be substantially lower than the MV-assisted systems. At all concentrations of DQ^{2+}, and in some concentrations for MV^{2+}, FEs lower than 100% were observed. Such behavior has been tentatively ascribed previously to complications associated with possible mediator dimerization[11,48] to generate a minimally competent electron donor. It is conceivable that the lower driving force in electron transfer of $DQ^{\bullet+}$ allows the radical to be present at substantial concentration and in close proximity within the MOF pores, for a longer duration than $MV^{\bullet+}$ to enhance the dimerization. Shown in Figure 4d is the dependence of TOF values for MV^{2+}-mediated hydrogen evolution as a function of pH. The values are derived from measurements of amounts of H_2 formed during electrolysis at −420 mV vs. RHE. The observed increases in TOF with increasing proton activity suggest that the rate-determining step(s), at least at E = −420 mV, involve a proton-coupled processes. From the previous mechanistic work,[15–16] we believe the rate-determining step(s) culminate in molybdenum-hydride formation. Notably, at all pH values examined the TOF value for catalysis of hydrogen formation by **MoS_x-SIM-NDC-SALI** proved to be lower than that for NDC-free **MoS_x-SIM**.

Solvent/electrolyte kinetic isotope effects (KIEs) indicate a possible dependence of the RDS(s) on the applied potential. Comparisons of catalytic currents recorded in pH 1.2 H_2SO_4 vs. pD 1.2 D_2SO_4 reveal a gradual change in KIE from close to 1 near the foot of the catalytic wave to above two at potentials negative enough to reach the top of the catalytic wave; see Figures S10b–c. In line with previous findings for NDC-free **MoS_x-SIM** as the electrocatalytic, these results imply little or no participation of protons in the RDS at the less negative potentials associated with the foot of the catalytic wave, but increasing participation at more negative potentials, with H/D KIE values exceeding 2 in the plateau region of the catalytic waves.

2.3.1. Foot-of-the-wave Analysis

The foot-of-the-wave analysis (FOWA) method developed by Savéant and co-workers[49] allows second-order rate constants (k) and the TOF as a function of applied overpotential (η) to be deduced from CVs. We extended our previous application of FOWA in a RM-assisted electrocatalytic system to the presented work, where the cathodic peak current in the absence of a substrate (a value non-intuitive to derive for HER in an aqueous system) is attributed to the RM reduction using the similar, but non-catalytic system, the oxide derivative, as the electrode; see the reference for details.[11] With this, the second-order rate constants specific to a given RM^{2+}, k_{RM}, were derived for **MoS_x-SIM-NDC-SALI**. As shown in Figures 5a and b and Table 1, k_{RM} of **MoS_x-SIM-NDC-SALI** are (a) higher for MV-assisted system than the DQ-assisted system and (b) lower when NDC is incorporated within the framework as compared to the framework in which it is absent, in agreement with the TOF measurements. From the k_{RM} values, plots of TOF *vs.* overpotential (η) plots were generated. Notably, the TOF at zero overpotential (denoted TOF_0) is higher for the DQ-assisted system than the MV-assisted analogue, in contrast to the ordering of in k_{RM} values. As explained previously,[11] at η = 0 V vs. RHE, $DQ^{\bullet+}$ exists in substantially larger concentration than $MV^{\bullet+}$ – a consequence of its ~80 mV more positive E_f; this difference is enough to offset the larger driving force for $MV^{\bullet+}$ (vs. $DQ^{\bullet+}$) electron transfer to the catalyst. For both mediators, NDC incorporation again lowers the calculated TOF_0; see Figure 5c and Table 1.

Table 1. Second-order rate constants and TOF at zero over potential of **MoS_x-SIM-NDC-SALI** and that without NDC in the presence of MV^{2+} or DQ^{2+} in pH 1.2 H_2SO_4.

Catalyst	Redox mediator	k_{RM} [$M^{-1}s^{-1}$]	TOF_0 [$\times 10^{-3}$ min^{-1}]
MoS_x-SIM-NDC-SALI	MV^{2+}	31 ± 5	1.7
MoS_x-SIM-NDC-SALI	DQ^{2+}	17 ± 1	19
MoS_x-SIM[a]	MV^{2+}	36 ± 8	2.8
MoS_x-SIM[a]	DQ^{2+}	23 ± 3	36

[a] These values were measured with the exactly identical electrode fabrication as to the NDC-SALI-derivative to be consistent.

© 2019 Wiley-VCH Verlag GmbH & Co. KGaA, Weinheim

21960216, 2020, 2, Downloaded from https://chemistry-europe.onlinelibrary.wiley.com/doi/10.1002/celc.201901650 by Chung-Ang University, Wiley Online Library on [26/11/2024]. See the Terms and Conditions (https://onlinelibrary.wiley.com/terms-and-conditions) on Wiley Online Library for rules of use; OA articles are governed by the applicable Creative Commons License

21960216, 2020, 2, Downloaded from https://chemistry-europe.onlinelibrary.wiley.com/doi/10.1002/cetc.201901650 by Chung-Ang University, Wiley Online Library on [26/11/2024]. See the Terms and Conditions (https://onlinelibrary.wiley.com/terms-and-conditions) on Wiley Online Library for rules of use; OA articles are governed by the applicable Creative Commons License

2.4. Pore Environment Effects: MoS_x-SIM-NDC-SALI vs. MoS_x-SIM

Consistent with their presentation of catalyst active-sites whose local structures are identical, the electrocatalytic behavior of **MoS_x-SIM-NDC-SALI** closely parallels that of **MoS_x-SIM**. Nevertheless, for a broad range of conditions, TOFs and catalytic currents are smaller (typically by a factor of two or so) for **MoS_x-SIM-NDC-SALI** relative to **MoS_x-SIM** as the electrocatalytic material. The most salient difference between the two is the siting of roughly a third of the $Mo(SH)_2$ units of **MoS_x-SIM** in the small *c*-pore (with the balance sited at the perimeter of the mesopore) versus siting $Mo(SH)_2$ units in **MoS_x-SIM-NDC-SALI** exclusively in mesopores. The combined results point to a significant local-environment effect upon catalyst performance. If the observed factor-of-two differences (roughly) in catalytic efficacy for the two materials are ascribed entirely to the fraction active-sites anchored in *c*-pores, *i.e.* if active-sites in mesopores are assumed to function identically in **MoS_x-SIM-NDC-SALI** vs. NDC-free **MoS_x-SIM**, we can infer that *otherwise identical $Mo(SH)_2$ units are roughly four times more active when sited in the MOF c-pore than in the mesopore.*

It is tempting to point to favorable water or hydronium-ion mediated hydrogen-bonding interactions between *c*-pore node-ligated aqua and/or hydroxo ligands and opposite-node-sited catalyst active-sites ($Mo(SH)_2$ units). Corroboration and mechanistic elucidation will likely require complementary computational-modeling studies. Regardless, it remains to be seen whether the putative favorable hydrogen-bonding interactions are most relevant for the catalyst resting state, a molybdenum-hydride-containing catalyst intermediate state, or a catalyst-enabled, reaction transition-state.

3. Conclusions

NDC incorporation converts NU-1000 from an eight-connected Zr-MOF to a ten-connected Zr-MOF and eliminates micropores as potential binding sites for single-metal-atom HER catalysts. As such, the catalyst-functionalized material, **MoS_x-SIM-NDC-SALI**, constitutes an extended porous array of redox-mediator-addressable *single-site* catalysts. Single-crystal X-ray structural data confirm both the single-site and single-metal-atom nature of the catalytic moiety, *i.e.* node-grafted $Mo(SH)_2$. We find that the array is electrocatalytically competent for evolution of molecular hydrogen from aqueous acid. Based on measurements of catalytic currents, TOFs, and/or mediator-catalyst ET rate constants as function of proton activity, mediator concentration, mediator formal potential solvent + electrolyte isotope (H/D) composition, and applied electrochemical potential, we find that **MoS_x-SIM-NDC-SALI** behaves in mechanistically similar fashion to NDC-free **MoS_x-SIM**, reported previously.[11] Namely, when both systems are subjected to electrochemical potentials that are sufficiently reducing, RM-assisted electron transfer(s) and proton-dependent step(s) are similar in rate. As such, they collectively dictate and control the overall reaction rate. This behavior can be contrasted with the perhaps more familiar case where a single RDS defines the overall reaction rate. Nevertheless, the catalytic activity of **MoS_x-SIM-NDC-SALI** – as indicated by catalytic currents and direct assessment of TOFs for H_2 production – is consistently less than that of **MoS_x-SIM**, typically by about a factor of two. The difference translates into an apparent four-fold greater degree of catalytic activity for Mo $(SH)_2$ units sited in micropores vs. mesopores. We speculatively ascribe the difference to kinetically beneficial hydrogen-bond-networking across the narrow (<10 Å) micropores. Regardless, the observed differences underscore the value of obtaining and working with heterogeneous electrocatalysts characterized by both active-site uniformity, and uniformity of the chemical environment beyond the active-site.

Experimental Section

Electrode Fabrication and Catalytic Testing

All MOF-based samples were synthesized according to reported procedures.[11,38,40,42] Electrode fabrication is analogous to that reported previously.[11] Briefly, 10 mg of MOF samples were suspended in 1 mL of ethanol that was dried with $MgSO_4$ prior to the addition. The suspension was briefly sonicated and 3 μL of the suspension was drop-casted onto an FTO substrate where the electroactive area was controlled to be 0.25 cm^2 using an electrically insulating polyamide tape. Once the film had dried, it was used as the working electrode in a standard H-cell set-up with septum to seal the headspace gas for gas chromatography (GC) measurements, with a Pt coil and Ag/AgCl (3 M) as the counter and reference electrodes, respectively. The electrolyte was purged with N_2 for at least 20 minutes prior to any electrochemical measurement. After bulk electrolysis, 200 μL of the working electrode chamber headspace gas was injected into the GC. For details on the GC set-up, see the reference.[8] All sulfide-based electrodes were prepared in an argon-filled glovebox and the dried ethanol used for the suspension was purged with N_2 for 20 minutes prior to the addition to prevent excessive oxidation.

Acknowledgments

This work was supported as part of the Center for Light Energy Activated Redox Processes (LEAP), an Energy Frontier Research Center funded by the U.S. Department of Energy, Office of Science, Basic Energy Sciences under Award #DE-SC0001059. H.N. gratefully acknowledges support from the Ryan Fellowship program of the Northwestern University International Institute of Nanotechnology. Z.L. acknowledges the support from the National Natural Science Foundation of China (Grant No. 21601047). This material is based upon work supported by the National Science Foundation Graduate Research Fellowship under Grant No. (DGE-1842165) (Z.H.S.). This work made use of the J. B. Cohen X-ray Diffraction, EPIC, IMSERC, and KECK II facilities of Northwestern University's NUANCE Center, which has received support from the Soft and Hybrid Nanotechnology Experimental (SHyNE) Resource (NSF ECCS-1542205); the MRSEC program (NSF DMR1720139) at the Materials Research Center; the Institute for Nanotechnology (IIN); the Keck Foundation; and the State of Illinois, through the IIN. MRCAT operations are supported by the Department of Energy and the MRCAT member

© 2019 Wiley-VCH Verlag GmbH & Co. KGaA, Weinheim

institutions. This research used resources of the Advanced Photon Source, a U.S. Department of Energy (DOE) Office of Science User Facility operated for the DOE Office of Science by Argonne National Laboratory under Contract No. DE-AC02-06CH11357. Finally, J.T.H. acknowledges Dick Crooks' scientific influence upon his own work, and Dick's friendship and professional kindness over the years. Congratulations, Dick, on an impressive and accomplished lifetime of professional mentoring and scholarly contributions.

Conflict of Interest

The authors declare no conflict of interest.

Keywords: molybdenum sulfide · metal**organic framework · hydrogen evolution reaction · electrocatalysis · redox mediator

[1] M. E. Dry, *Catal. Today* **2002**, *71*, 227–241.
[2] H. Jahangiri, J. Bennett, P. Mahjoubi, K. Wilson, S. Gu, *Catal. Sci. Technol.* **2014**, *4*, 2210–2229.
[3] A. Y. Khodakov, W. Chu, P. Fongarland, *Chem. Rev.* **2007**, *107*, 1692–1744.
[4] J. W. Erisman, M. A. Sutton, J. Galloway, Z. Klimont, W. Winiwarter, *Nat. Geosci.* **2008**, *1*, 636–639.
[5] T. Kandemir, M. E. Schuster, A. Senyshyn, M. Behrens, R. Schlögl, *Angew. Chem. Int. Ed.* **2013**, *52*, 12723–12726; *Angew. Chem.* **2013**, *125*, 12955–12959.
[6] J. M. Ogden, *Annu. Rev. Energ. Environ.* **1999**, *24*, 227–279.
[7] N. S. Lewis, D. G. Nocera, *Proc. Mont. Acad. Sci.* **2006**, *103*, 15729–15735.
[8] H. Noh, Y. Yang, S. Ahn, A. W. Peters, O. K. Farha, J. T. Hupp, *J. Electrochem. Soc.* **2019**, *166*, H3154-H3158.
[9] D. Zeng, T. Zhou, W.-J. Ong, M. Wu, X. Duan, W. Xu, Y. Chen, Y.-A. Zhu, D.-L. Peng, *ACS Appl. Mater. Interfaces* **2019**, *11*, 5651–5660.
[10] M. Ni, M. K. H. Leung, D. Y. C. Leung, K. Sumathy, *Renewable Sustainable Energy Rev.* **2007**, *11*, 401–425.
[11] H. Noh, C.-W. Kung, K.-I. Otake, A. W. Peters, Z. Li, Y. Liao, X. Gong, O. K. Farha, J. T. Hupp, *ACS Catal.* **2018**, *8*, 9848–9858.
[12] M. Zeng, Y. Li, *J. Mater. Chem. A* **2015**, *3*, 14942–14962.
[13] Q. Ding, B. Song, P. Xu, S. Jin, *Chem* **2016**, *1*, 699–726.
[14] E. Skúlason, V. Tripkovic, M. E. Björketun, S. Gudmundsdóttir, G. Karlberg, J. Rossmeisl, T. Bligaard, H. Jónsson, J. K. Nørskov, *J. Phys. Chem. C* **2010**, *114*, 18182–18197.
[15] C. Tsai, K. Chan, F. Abild-Pedersen, J. K. Norskov, *Phys. Chem. Chem. Phys.* **2014**, *16*, 13156–13164.
[16] X. Zou, Y. Zhang, *Chem. Soc. Rev.* **2015**, *44*, 5148–5180.
[17] T. F. Jaramillo, K. P. Jørgensen, J. Bonde, J. H. Nielsen, S. Horch, I. Chorkendorff, *Science* **2007**, *317*, 100–102.
[18] J. D. Benck, T. R. Hellstern, J. Kibsgaard, P. Chakthranont, T. F. Jaramillo, *ACS Catal.* **2014**, *4*, 3957–3971.
[19] J. D. Benck, Z. Chen, L. Y. Kuritzky, A. J. Forman, T. F. Jaramillo, *ACS Catal.* **2012**, *2*, 1916–1923.
[20] P. D. Tran, V. Tran, M. Orio, S. Torelli, Q. D. Truong, K. Nayuki, Y. Sasaki, Y. Chiam, R. Yi, I. Honma, J. Barber, V. Artero, *Nat. Mater.* **2016**, *15*, 640.
[21] J.-H. Li, Y.-S. Wang, Y.-C. Chen, C.-W. Kung, *Appl. Sci.* **2019**, *9*.
[22] T. Islamoglu, S. Goswami, Z. Li, A. J. Howarth, O. K. Farha, J. T. Hupp, *Acc. Chem. Res.* **2017**, *50*, 805–813.
[23] X. Gong, H. Noh, N. C. Gianneschi, O. K. Farha, *J. Am. Chem. Soc.* **2019**, *141*, 6146–6151.
[24] H. Noh, C.-W. Kung, T. Islamoglu, A. W. Peters, Y. Liao, P. Li, S. J. Garibay, X. Zhang, M. R. DeStefano, J. T. Hupp, O. K. Farha, *Chem. Mater.* **2018**, *30*, 2193–2197.
[25] K.-I. Otake, Y. Cui, C. T. Buru, Z. Li, J. T. Hupp, O. K. Farha, *J. Am. Chem. Soc.* **2018**, *140*, 8652–8656.
[26] K.-I. Otake, J. Ye, M. Mandal, T. Islamoglu, C. T. Buru, J. T. Hupp, M. Delferro, D. G. Truhlar, C. J. Cramer, O. K. Farha, *ACS Catal.* **2019**, *9*, 5383–5390.
[27] J. Lyu, X. Zhang, K.-I. Otake, X. Wang, P. Li, Z. Li, Z. Chen, Y. Zhang, M. C. Wasson, Y. Yang, P. Bai, X. Guo, T. Islamoglu, O. K. Farha, *Chem. Sci.* **2019**, *10*, 1186–1192.
[28] X. Zhang, Z. Huang, M. Ferrandon, D. Yang, L. Robison, P. Li, T. C. Wang, M. Delferro, O. K. Farha, *Nat. Can.* **2018**, *1*, 356–362.
[29] The alternating Mo1 and Mo3 pattern shown in Figure 1b is simply for clarity and does not represent the statistical distribution between the two species resided within the mesopore. Further for clarity, Figure 1b only shows Mo1 and Mo3 within a single hexagonal channel, but these species reside within all hexagonal channels.
[30] Figure 1c shows only one of the two hydroxyl/aqua groups on the node pointing into the microporous c-pore to be occupied by the Mo(SH) 2 units as statistically, this is the most likely confirmation as to where two or zero Mo(SH)2 units occupy the deposition sites, given the average Mo(SH)2 units loading per node of 2.6. We can, however, not rule out the existence of the latter two cases.
[31] J. E. Mondloch, W. Bury, D. Fairen-Jimenez, S. Kwon, E. J. DeMarco, M. H. Weston, A. A. Sarjeant, S. T. Nguyen, P. C. Stair, R. Q. Snurr, O. K. Farha, J. T. Hupp, *J. Am. Chem. Soc.* **2013**, *135*, 10294–10297.
[32] N. Planas, J. E. Mondloch, S. Tussupbayev, J. Borycz, L. Gagliardi, J. T. Hupp, O. K. Farha, C. J. Cramer, *J. Phys. Chem. Lett.* **2014**, *5*, 3716–3723.
[33] A. Peters, Z. Li, O. K. Farha, J. T. Hupp, *ACS Appl. Mater. Interfaces* **2016**, *8*, 20675–20681.
[34] Z. Li, A. W. Peters, A. E. Platero-Prats, J. Liu, C. W. Kung, H. Noh, M. R. DeStefano, N. M. Schweitzer, K. W. Chapman, J. T. Hupp, O. K. Farha, *J. Am. Chem. Soc.* **2017**, *139*, 15251–15258.
[35] S. Ahn, S. L. Nauert, C. T. Buru, M. Rimoldi, H. Choi, N. M. Schweitzer, J. T. Hupp, O. K. Farha, J. M. Notestein, *J. Am. Chem. Soc.* **2018**, *140*, 8535–8543.
[36] P. Ji, K. Manna, Z. Lin, X. Feng, A. Urban, Y. Song, W. Lin, *J. Am. Chem. Soc.* **2017**, *139*, 7004–7011.
[37] P. Ji, K. Manna, Z. Lin, A. Urban, F. X. Greene, G. Lan, W. Lin, *J. Am. Chem. Soc.* **2016**, *138*, 12234–12242.
[38] H. Noh, Y. Cui, A. W. Peters, D. R. Pahls, M. A. Ortuño, N. A. Vermeulen, C. J. Cramer, L. Gagliardi, J. T. Hupp, O. K. Farha, *J. Am. Chem. Soc.* **2016**, *138*, 14720–14726.
[39] As outlined in ref. 38, SIM typically consists of three processes: (1) submerging bulk MOF powders typically for an overnight in a solution of metal precursor in an inert solvent (e.g., heptane), (2) extensive washing with the solvent to remove excess, uncoordinated metal precursors, (3) thermal activation to remove solvent from MOF pores.
[40] A. W. Peters, K. Otake, A. E. Platero-Prats, Z. Li, M. R. DeStefano, K. W. Chapman, O. K. Farha, J. T. Hupp, *ACS Appl. Mater. Interfaces* **2018**, *10*, 15073–15078.
[41] SALI follows a similar process as to SIM where bulk MOF powders are soaked in a solution of ligand (typially solubilized in dimethylformamide). See ref. 40 for more details.
[42] T. Islamoglu, K.-I. Otake, P. Li, C. T. Buru, A. W. Peters, I. Akpinar, S. J. Garibay, O. K. Farha, *CrystEngComm* **2018**, *20*, 5913–5918.
[43] Y. Okamoto, N. Oshima, Y. Kobayashi, O. Terasaki, T. Kodaira, T. Kubota, *Phys. Chem. Chem. Phys.* **2002**, *4*, 2852–2862.
[44] I. Lezcano-González, R. Oord, M. Rovezzi, P. Glatzel, S. W. Botchway, B. M. Weckhuysen, A. M. Beale, *Angew. Chem. Int. Ed.* **2016**, *55*, 5215–5219; *Angew. Chem.* **2016**, *128*, 5301–5305.
[45] M. Kertesz, R. Hoffmann, *J. Am. Chem. Soc.* **1984**, *106*, 3453–3460.
[46] C. L. Bird, A. T. Kuhn, *Chem. Soc. Rev.* **1981**, *10*, 49–82.
[47] The FE with no redox mediator was measured to be substantially lower as evident from Figure S8. As revealed in Figure S5, even a bare FTO gave rise to similar current despite no detectable hydrogen formation. Thus, we believe this background current that yields no hydrogen is substantially decreasing the apparant FE.
[48] J. W. Park, N. H. Choi, J. H. Kim, *J. Phys. Chem.* **1996**, *100*, 769–774.
[49] C. Costentin, S. Drouet, M. Robert, J.-M. Savéant, *J. Am. Chem. Soc.* **2012**, *134*, 11235–11242.

Manuscript received: October 2, 2019
Revised manuscript received: December 18, 2019
Accepted manuscript online: December 31, 2019

© 2019 Wiley-VCH Verlag GmbH & Co. KGaA, Weinheim

21960216, 2020, 2, Downloaded from https://chemistry-europe.onlinelibrary.wiley.com/doi/10.1002/celc.201901650 by Chung-Ang University, Wiley Online Library on [26/11/2024]. See the Terms and Conditions (https://onlinelibrary.wiley.com/terms-and-conditions) on Wiley Online Library for rules of use; OA articles are governed by the applicable Creative Commons License